Galaxy Cluster Dynamics in the Era of Large Spectroscopic Surveys

Steven Boada

July 30, 2015

1 Introduction

Clusters of galaxies form the largest bound objects in the universe, and as such their study is a cornerstone in modern day astronomy. First recognized by 19th century astronomers, their place in astronomical canon was solidified when Edwin Hubble proofed their constituent nebulae where not bound to the Milky Way (Hubble 1926) but collections of stars similar to the Milky Way. Work to understand their nature and origin began in ernest when Hubble & Humason (1931) used the virial theorem and the galaxy velocities in the centers of the Virgo (Smith 1936) and Coma (Zwicky 1933) clusters to derive their masses. The immense mass derived exceeded the total stellar mass contributed by all galaxies many times over. This lead Zwicky to theorize the existence of large amounts of non-luminous matter, and coining the term "dark matter" (DM), which we still use today.

Modern astronomy gives the composition of galaxy clusters in three many parts. The galaxies themselves comprise the most obvious feature, and contain a large portion (but not the entirety) of the luminous matter (stars) in the cluster. The intracluster medium (ICM) is the space between the cluster galaxies and is composed many of ordinary matter (baryons) which are super heated to tens of thousands of kelvin. The ICM contains the bulk of the cluster's baryonic matter, and while it is very hot, it is not very dense, with a typical value of 10^{-3} particles per cubic centimeter. The majority of the cluster's mass is located in the DM halo which surrounds the cluster.

Thought to form out of the primordial density fluctuations in the very early universe, the investigation of their formation and growth began in the 1960s. Soon thereafter, the hierarchical model of structure formation (Press & Schechter 1974; Gott & Rees 1975; White & Rees 1978) was introduced. It suggests the first stars and stellar clumps grew first then subsequently merged together with dark matter and other gas clumps to form the first galaxies which then continued to merge and grow into the clusters and large scale structures we see today. This accretion of smaller systems is thought to be driven by the gravity of the DM associated with the cluster. Of course, many complicated astrophysical processes are at work during cluster growth and similarly complicated theoretical models seek to explain these processes. For a detailed review of cluster formation see Kravtsov & Borgani (2012).

The number and distribution of galaxy clusters across the sky is the finger print of the cosmology imprinted on the universe at its birth. To uncover the underlying cosmology a detailed understanding of the astrophysical processes that describe the motion of constituent galaxies and their impact on the ICM is required. So, galaxy clusters stand at the intersection of cosmology and astrophysics.

1.1 Cluster Cosmology

The current concordance cosmology is a parametrization of the Big Bang cosmological model where the universe contains a cosmological constant (Λ; often referred to as dark energy) and cold dark matter (CDM). It is often characterized by six parameters; the Hubble Constant (H_0), the baryonic matter density (Ω_b), the dark matter density (Ω_c), the dark energy density (Ω_Λ); the normalization of the power spectrum (σ_8); the spectral index of the power spectrum (n_s). Galaxy clusters are sensitive probes of Ω_m, the total mass ($\Omega_b + \Omega_c$) density in the universe, through tracing the peaks in the universal matter density often referred to as the power spectrum of matter density fluctuations or the matter power spectrum and σ_8 by the comparison of the number density of observed halos to that predicted in cosmological models.

The determination of cosmological parameters is done by comparing the number of galaxy clusters per unit mass per unit comoving volume ($n(M, z)$) to models. See Allen et al. (2011) for a comprehensive review or Murray et al. (2013) for a more practical approach. $n(M, z)$, referred to as the halo mass function (HMF) captures the number evolution through a function which defines the particular model used. Early work by Press & Schechter (1974) and Bond et al. (1991) which assumed spherical halos, have largely been replaced by more modern fitting functions which, at the expense of an analytical solution, provide more accurate results when fit to simulation data. See Murray et al. (2013) for a review of the most common fitting functions used. Through this approach, the two parameters which clusters are most sensitive to, Ω_m and σ_8 are in reality measured as $\sigma_8\Omega_m^\alpha$, where the value of α depends on the masses of the halos considered. The degeneracy is broken through the evolution of the HMF as a function of redshift.

The ΛCDM model of cosmology makes explicit predictions about the number and masses of galaxy clusters throughout the universe. Connecting these predictions to a set of, sufficiently large in size, observed clusters remains a principal problem. Specifically, the largest threat to modern, precision, cluster cosmology is not the identification of large numbers of clusters (the total number of clusters known is only going up) but the accurate recovery of galaxy cluster mass. This problem extends to both the very rich clusters (those with high mass) and, importantly, the poor clusters (those with low mass) as the relationship between galaxy cluster mass and many of the observables which trace mass is not well understood for such low mass clusters.

1.2 State of Play

As mass is not a direct observable, a lot of work is underway to characterize galaxy cluster masses with an observable feature of galaxy clusters. In this section, we will briefly touch on a few of the ways cluster mass is determined, and address any short comings the method may have. Generally, the methods fall into two distinct camps, simulation based and direct or statistical calibration. The goal is to constrain, as best possible, $P(X|M, z)$ or the probability (P) that a galaxy cluster of given mass (M) located at redshift (z) using observable parameter (X).

One could use various simulations to attempt to calibrate this observable–mass relation (e.g., Vanderlinde et al. 2010; Sehgal et al. 2011). However, the primary challenge to this method is the incomplete understanding of the baryonic physics which take place in galaxy cluster environments. While there have been (and continue to be) many improvements in the accuracy and power of simulations it is doubtful that in the coming years they will reach the accuracy level required to the point where the observable–mass relation is dominated only by statistics (Weinberg et al. 2013).

The second broad camp is the direct calibration of cluster masses. This recipe has two distinct but not always independent tracks. The "direct" method uses the direct observations of a small set of clusters and then uses known mass estimators, X-ray hydrostatic or weak lensing (WL) as examples, which provide a "true" mass. This directly calibrates the observable–mass relation which is then applied to a much larger sample. The complications lie in that the "true" masses are in fact estimations, and the methods used to recover these masses are subject to their own limitations. X-ray hydrostatic estimations assume hydrostatic equilibrium which may only be valid for a very small number and range of cluster masses. The Sunyaev–Zeldovich (SZ; Sunyaev & Zeldovich 1972) effect, which uses the up–scattering of cosmic microwave background (CMB) photons to estimate cluster masses, provides accurate estimations of mass, but the ability to detect low mass galaxy clusters is currently limited by technology. WL estimates are, in principle, correct in the mean, but they suffer from signal-to-noise requirements, limiting their usefulness in low mass clusters, and potentially suffer from line-of-sight effects as the effect is sensitive to all mass along the line of sight. Virial mass estimators which determine the cluster mass based on the motions of the member galaxies is promising in that it is a direct measurement of the depth of clusters potential well, but suffers from systematics due to cluster formation physics which disrupts the velocity field.

The statistical method of determining galaxy cluster mass relies not on direct measurements of individual clusters but the calibration of observables for the entire sample which correlate with cluster mass. One example is the spatial clustering of the galaxy clusters themselves. See Weinberg et al. (2013) for a comprehensive review. In practice, it will be a combination of the three methods touched on that will provide the most reliable determination of cluster masses.

Virial mass estimators, specifically, can be applied in both a direct and statistical fashion. Currently, the accuracy of such a method, especially to the level required for today's precision cosmology, is not well constrained. In the coming years large spectroscopic surveys will

provide enough coverage, and so these methods warrant further investigation (e.g., Saro et al. 2013).

1.3 Cluster Surveys in the near-future

In the coming years, many large surveys will add further statistical advantages to the determination of cosmological parameters using galaxy clusters.At their completion, the South Pole Telescope (SPT) and the Atacama Cosmology Telescope (ACT) are expected to find approximately one thousand clusters using observations in the millimeter combined with the SZ effect. Attempts are already underway to calibrate these observations using subsamples of clusters (approximately 100 cluster candidates and 60 clusters respectively) and other observables such as virial estimates or X-ray temperature measurements (e.g., Sifón et al. 2013; Bocquet et al. 2015).

X-ray identified clusters, up until today, have mostly been observed fortuitously through targeted *Chandra* or *XMM-Newton* observations. That is soon to change with the *eROSITA* telescope onboard the Spektrum-Roentgen-Gamma Mission, which will perform an all–sky survey during its four year mission and detect an estimated 50,000 or more clusters.

Large optical surveys such as the Dark Energy Survey (DES; The Dark Energy Survey Collaboration 2005) and the Large Synoptic Survey Telescope (LSST) will survey enormous portions of the sky extremely deeply and will identify vast numbers of clusters using optical selection methods (e.g., Rykoff et al. 2014; Rozo et al. 2014). However, the majority of these surveys will be photometric, and any spectral information will be obtained from preexisting datasets. And while it is possible to estimate cluster masses using photometric redshifts, primarily through the richness–mass relation, (e.g., Rykoff et al. 2012, 2014), spectroscopic followup is required to both better calibrate the relation and to obtain the level of precision needed to compete with other mass estimators.

1.4 Impact of This Work

As the sample of known clusters grows to many tens of thousands, spectroscopic followup becomes unfeasible. Large spectroscopic surveys will be required to reduce systematics to a level that will allow accurate mass estimations using virial methods. The Hobby Eberly Dark Energy Experiment (HETDEX; Hill et al. 2008b) is a forthcoming blind spectroscopic survey that could potentially be used to accurately calibrate the observable–mass relation for a significant number of galaxy clusters at both extremes of the mass scale. HETDEX is designed to measure the dark energy equation of state at $z \sim 2$, and so the applicability to galaxy cluster science has not yet been investigated.

Given how much progress could be made with HETDEX, this work seeks to address this issue in two ways. First, using a set of state-of-the-art simulations we will simulate the observing strategy of HETDEX to determine the number and nature of clusters that might be observed. See Section 2. This is done in four distinct ways and in each part we will measure the dynamical properties, such as redshift, LOSVD, and mass of the clusters. First we

will use targeted observations and perfect knowledge of the observed galaxy clusters, which includes center, membership, and number to recover the desired properties. Secondly, we will assume that we know the location but not the center, membership, or number of constituent galaxies. Then we will employ the HETDEX observing strategy, including realistic pointing pattern, observational magnitude constraints, and spectral sensitivity limits to generate a set of realistic observations which are then used with perfect and less than perfect knowledge scenarios to determine the cluster properties.

In all cases, we will attempt to characterize the observable–mass relation (or relations) to better understand the dominate sources of uncertainty when using HETDEX like observations. This will enable us to more fully understand and constrain the HMF which, in turns, allows us to make more accurate measurements of the cosmological parameters traced by galaxy clusters.

The second effort of this work, outlined in Section 3, will use targeted spectroscopic observations of ten nearby clusters with the Mitchell Spectrograph (formerly known as VIRUS-P; Hill et al. 2008a), an integral field unit (IFU) in a square array of 246 4.24″ diameter optical fibers, to test some of the methods used in the first method. This will provide insight in how the observable–mass relation may be improved through followup observations of targeted clusters.

2 Cluster Dynamics Using the Hobby Eberly Telescope Dark Energy Experiment

2.1 Introduction

I. Introduction

A. The goal of this project is to investigate how well we are able to recover the observable–mass relation. The observable will be either the richness or the line-of-sight velocity dispersion (LOSVD). We will use two different observation strategies and two different scenarios for each strategy. The first will use targeted observations of clusters which will select all galaxies within a radius of the cluster center. The second observing technique will use HETDEX like observations, including pointing pattern, to observe clusters. In each case, first perfect information, including cluster center and galaxy membership will be use to derive the cluster masses. Secondly, more realistic conditions where the cluster center and membership are not precisely known will be used to derive the masses. We will be able to better understand the observational conditions effecting the accurate recovery of galaxy cluster masses.

2.2 Data and Observations

I. The “Aardvark Catalogs”

A. The "Aardvark" mock galaxy catalogs (R. Wechsler et al., private communication) are derived from a semi-analytical model (SAM) tied to an in house n-body cosmological simulation and designed for DES. They provide a 10313 degree^2(one quarter of the sky) catalog to full DES depth and contains 1.36 billion galaxies which have a signal-to-noise of at least five in one or more DES observing bands.

II. [O II] Luminosity

A. Need to make HETDEX-like observations. Because HETDEX is designed to find Lyα emitting galaxies, we are interested in [O II] emitters at a lower redshift. The simulations do not include emission line information so we must assign it.

B. [O II] luminosities are assigned empirically to aardvark galaxies by relating the M_r and $g-r$ color of 503113 galaxies selected from the SDSS to their measured [O II] line flux.

III. Mock Observations

A. Our "observations" consist of placing masks, which accurately recreate the HETDEX IFU layout, onto the aardvark catalogs and selecting all, $z < 0.5$ galaxies which meet the sensitivity limits lying underneath.

B. Sensitivity limits for HETDEX are 22 mag in SDSS g for galaxies $z < 0.4$ and [O II] line flux at least 3.5×10^{-17} erg s^{-1} cm^{-2} for $0.4 < z < 0.5$ galaxies.

2.3 Analysis

I. Cluster Membership

A. The number of cluster members is determined in two ways. For clusters with at least twenty members we using the "shifting gapper" method defined in Fadda et al. (1996). This method examines the velocity gaps between galaxies in similar spacial bins to identify members. The second method uses a spacial and velocity space cut to identify members when there are fewer than twenty observed galaxies. This method is outlined in Connelly et al. (2012) and Wilman et al. (2005).

II. Recovery of Cluster Parameters

A. Cluster Redshift

i. The cluster redshift is the average redshift of all cluster members. In practice this is determined by iterably determining the clusters members, updating the cluster redshift, and recomputing the members until convergence.

B. Line of Sight Velocity Dispersion

i. The line-of-sight velocity dispersion (LOSVD) is calculated by the biweight sample variance (Ruel et al. 2014) when there are at least fifteen members. For clusters with fewer than fifteen members we use the gapper estimator (Beers et al. 1990).

C. Dynamical Mass

i. The dynamical mass is determined by using the scaling relation of Munari et al. (2013) which has been used by several other observational studies. The relation determines a M_{200c}, the mass enclosed in a radius in which the density is 200 times the critical density of the Universe, by scaling the observed LOSVD.

2.4 Results

I. Calibrating the Observable-Mass Relation

A. LOSVD

i. The large sample of galaxies provided by HETDEX will allow important discussion about the probability a recovered mass will accurately reproduce the true mass.

B. Richness

i. Because the use of simulations provides perfect knowledge about which galaxy is a member (or not) of each cluster, we are able to assign each cluster accurate richnesses. This allows us to characterize the scatter in the richness–mass relation minimizing the uncertainties on both the inferred mass and observed richness.

3 The VIRUS-P Cluster Survey

We will measure the correlation between dynamical mass measured from the velocity dispersion and other mass estimators (e.g., the clusters in this sample have deep Chandra or XMM X-ray data). The 10 clusters studied here will be used to reduce the three dominant sources of systematic uncertainties on cosmological parameters derived from cluster counts: we will measure the absolute mass scale of the richness estimator; we will identify the correct central cluster galaxy combining the spatial and redshift information, and we will measure the scatter of the richnessmass relation, $\sigma_{M|\lambda}$.

3.1 Design

I. Target Selection

A. We select clusters at $z = 0.2 - 0.3$ from two samples. Optically selected clusters, covering a wide range of richnesses, are from Rykoff et al. (2012) using the

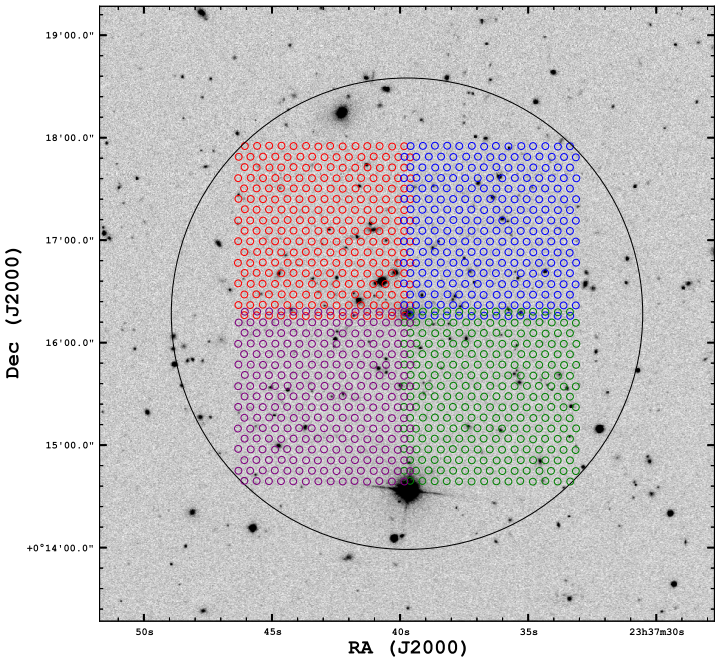

Figure 1: SDSS r-band image of an optically selected galaxy cluster selected from the SDSS DR8 data. The field is centered on the BCG, which has a measured spectroscopic redshift from SDSS of $z = 0.277$. The large black circle shows the region $R < 0.5$ Mpc ($r < 2.3'$). Nearly all galaxies within this region are associated with the cluster. The four MS fields (and fiber positions for the first dither position) are overdrawn on the field, illustrating how we survey each cluster.

Sloan Digital Sky Survey (SDSS; Blanton et al. 2001) Data Release 8 and with high richness corresponding to $M_{DM} > 8 \times 10^{14} M_{\odot}$. X-ray selected clusters are from the *XMM Cluster Survey* (XCS; Mehrtens et al. 2012) and have individually measured X-ray temperatures of $T_X < 2.5$keV and inferred masses $> 10^{14} M_{\odot}$.

II. The Mitchell Spectrograph

A. The Mitchell Spectrograph (formerly known as VIRUS-P; Hill et al. 2008a) is an integral field unit in a square array of 246 4.24″ diameter optical fibers.

III. Observations

A. The observations of all clusters were completed in the Spring of 2013.

B. We use the Mitchell Spectrograph (MS) to target the galaxy clusters using the 5Å grating covering a wavelength range of 4400 - 6600Å. After reducing all spectra we find a final instrumental resolution of $\sigma_{inst} = 146$ km s^{-1}, similar to that of other studies using the MS (e.g., Murphy et al. 2011; Blanc et al. 2013), and sufficient enough for the determination of cluster masses.

i. We have set exposure times to achieve spectra with signal-to-noise ratios (SNRs) ~ 3 per spectral element in the continuum for objects with g = 21.3 mag (which corresponds to approximately 0.2L* for cluster galaxies at $z = 0.2$).

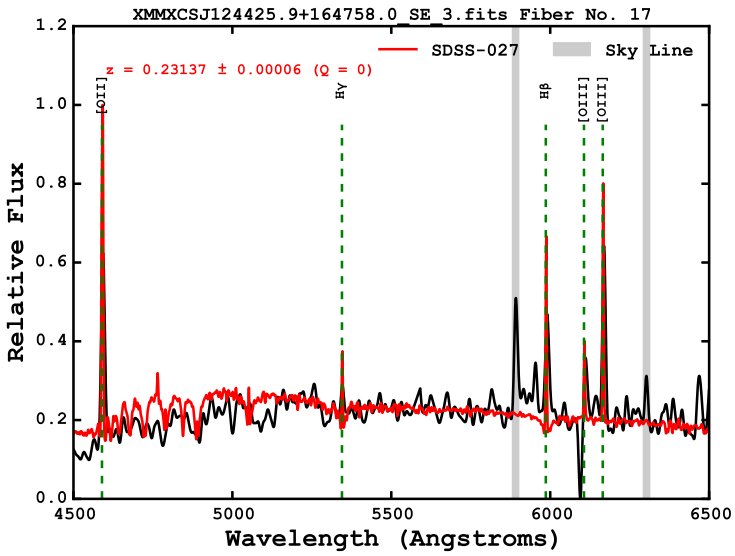

Figure 2: Example spectrum of an emission-line cluster galaxy (black line) and template fit (red line) from VIRUS-P on the McDonald 2.7m telescope. The spectrum shows the wavelength range and data quality expected from HETDEX-like spectroscopy, which are sufficient to measure galaxy redshifts.

3.2 Data Reduction

I. All data are reduced using P3D (Sandin et al. 2010) which is a general IFU reduction pipeline. It uses established techniques to both wavelength calibrate and extract the spectra. We do not flux calibrate our spectra.

II. We use wavelength calibration from images of Hg+Cd (for the May, 2012 observations) or Cd+Ne (for all subsequent observations) arc lamps.

III. The majority of fibers for any single pointing are empty, we use a 3σ clipped median selection to identify sky fibers and a simple average to combine them. The result is then subtracted from every fiber. This adequately removes the bulk of sky emission lines, but often fails to completely remove the O I line at 5577Å. This line is masked throughout the determination of redshifts. See Figure 2 for an example of a reduced spectrum.

3.3 Analysis

I. Redshift Catalog

A. A redshift solution is determined for each object by cross-correlating (Tonry & Davis 1979) each of the spectra with galaxy template spectra from the SDSS using the XCSAO task in the IRAF RVSAO package (Kurtz et al. 1992). See Figure 2 for an example of a fitted spectrum.

II. Photometric Catalog

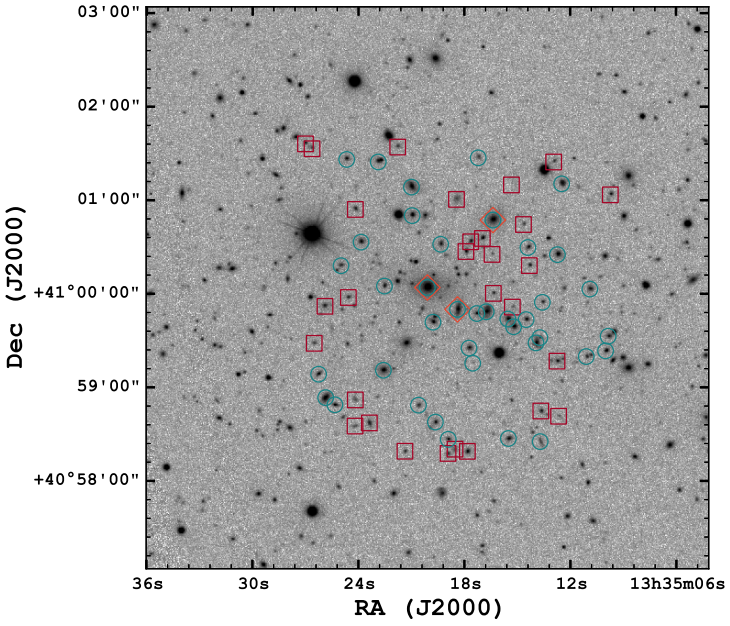

Figure 3: SDSS r image of cluster c203p83+41p0. The symbols show the position of observed galaxies. Blue circles indicate galaxies with $Q = 0$ or $Q = 1$ spectroscopic redshifts, red squares indicate galaxies where a redshift could not be reliably determined, and the orange diamond corresponds to galaxies with pre-existing redshifts from the SDSS.

A. Each galaxy detection has a corresponding SDSS detection providing photometric information in addition to the measured redshifts. See Figure 3 for an example of the spectroscopic targets matched to the photometric detections.

III. Data Quality Control

A. For each redshift computed a "Q" or quality flag is assigned. $Q = 0$ implies high-confidence redshifts, clearly determined by at least two obvious features. See Figure 2. Spectra with only a single strong feature (e.g., [O II] emission) but lie near the correct redshift of the cluster are assigned $Q = 1$ and redshifts resulting from enigmatic features are assigned $Q = 2$. For the determination of cluster properties we only consider $Q = 0$ and $Q = 1$ quality flags.

3.4 Results

I. Cluster Membership

A. To reject spurious sources not associated with the any given cluster we employ two methods. For clusters with 20 or more $Q = 0$ redshifts we use the "shifting gapped" method of Fadda et al. (1996).

B. For galaxy clusters with fewer than 20 $Q = 0$ redshifts we employ the method outlined in Connelly et al. (2012); Wilman et al. (2005) where we assume an initial velocity dispersion of 500km s^{-1} and apply both redshift and spatial limits. The number of total redshifts, $Q = 0$ redshifts, and confirmed cluster members are given in Table 1.

Table 1: Observed clusters with the total number of sources detected, the number of corresponding $Q = 0$ redshifts and the number of confirmed cluster members after the confirmation process has been completed. σ and M_{200} are very preliminary estimates of the LOSVD and dynamical mass. Clusters missing data have technical problems under current investigation.

Cluster	Sources	Q=0	Members	z_c	σ (km s^{-1})	M_{200} (10^{15} M$_\odot$)
c250p08+46p7	62	34	23	0.2256	1044^{+196}_{-131}	$1.75^{+0.6}_{-0.47}$
c203p83+41p0	68	39	26	0.2346	1364^{+241}_{-159}	$3.89^{+1.2}_{-0.96}$
c210p2+02p8	64	33	6	...	...	...
c234p2+24p4	38	24	19	0.2265	883^{+188}_{-91}	$1.06^{+0.40}_{-0.23}$
c260p61+32p13	61	42	26	0.2256	881^{+156}_{-93}	$1.05^{+0.34}_{-0.23}$
c16p23+0p06	42	24	17	0.2720	1215^{+228}_{-137}	$2.69^{+0.91}_{-0.64}$
c328p33+0p19	28	18	15	0.2165	396^{+120}_{-60}	$0.096^{+5.0}_{-3.2}$
c319p70+0p56	47	24	20	0.2760	729^{+142}_{-94}	$0.58^{+2.04}_{-1.60}$
XMMXCSJ124425.9+164758.0	24	12	6	0.2349	348^{+216}_{-109}	$0.06^{+5.56}_{-4.73}$
XMMXCSJ125650.2+254803.2	15	7	...	...	...	...

II. Cluster Redshift

A. The cluster redshift is the mean redshift of a confirmed member galaxies.

III. Line of Sight Velocity Dispersion

A. For clusters with at least 15 confirmed members we employ the biweight sample variance (Ruel et al. 2014) a modified version of the biweight scale estimator (Beers et al. 1990).

B. For galaxy clusters with fewer than 15 members, we employ the gapper estimator (Beers et al. 1990) which provides accurate dispersions for groups as small as 5 members (Hou et al. 2009).

IV. Dynamical Mass

A. We use a scaling relation from Evrard et al. (2008); Saro et al. (2013); Munari et al. (2013) to define the mass enclosed by r_{200c} which has been used in both simulations (e.g., Old et al. 2014), and observational studies (e.g., Brodwin et al. 2010).

3.5 Calibrating the Observable-Mass Relation

I. Richness

A. The dominant sources of error on these cosmological parameters from counts of optical clusters are systematic uncertainties on the absolute scale between the

cluster mass and optical richness, and the intrinsic scatter in cluster mass at fixed richness.

II. X-ray Temperature

A. Many (all) of the observed clusters also have X-ray observations. This will allow us a second independent check of the recovered halo masses.

4 Timeline to Completion

I. Spring 2015

A. April

i. Work using the Internal Color Dispersion is completed. Published, Boada et al. (2015).

B. May

i. HETDEX simulation analysis technical infrastructure is completed. This includes the code to replicate the HETDEX observations and all of the analysis code which calculates the derived quantities, LOSVD, mass, etc.

ii. Details outlining the methods used to derive these quantities are added to the paper draft.

iii. Details outline the chosen methods are also added to the VIRUS-P paper.

II. Summer 2015

A. June

i. Details of the direction of thesis work are hammered out.

B. July

i. Detailed direction of thesis is finalized.

ii. Analysis of HETDEX simulations begins in earnest.

iii. HETDEX paper is written concurrently with analysis.

C. August

i. Draft of HETDEX paper is completed and sent to co-authors.

ii. VIRUS-P data is sent through the already existing HETDEX analysis pipeline.

iii. Writing of the VIURS-P paper begins in earnest.

iv. Job search preparations begin.

D. September

i. HETDEX paper is submitted

ii. VIRUS-P paper is completed and sent to co-authors.

III. Fall 2015

A. October

i. VIRUS-P paper is submitted

ii. Begin dealing with HETDEX referee report

B. November

i. VIRUS-P referee report

ii. Resubmit HETDEX paper

IV. Winter 2015–2016

A. December

i. Resubmit VIRUS-P paper

B. January

i. Apply to Graduate

ii. Finish any outstanding issues with VIRUS-P paper

iii. Begin composing thesis

C. February

i. Write thesis

V. Spring 2016

A. March

i. Defend

B. April

i. Complete thesis

C. May

i. Graduate

References

Allen, S. W., Evrard, A. E., & Mantz, A. B. 2011, Annual Review of Astronomy and Astrophysics, 49, 409

Beers, T. C., Flynn, K., & Gebhardt, K. 1990, The Astronomical Journal, 100, 32

Blanc, G. a., Weinzirl, T., Song, M., et al. 2013, The Astronomical Journal, 145, 138

Blanton, M. R., Dalcanton, J., Eisenstein, D., et al. 2001, The Astronomical Journal, 121, 2358

Boada, S., Tilvi, V., Papovich, C., et al. 2015, The Astrophysical Journal, 803, 104

Bocquet, S., Saro, A., Mohr, J. J., et al. 2015, The Astrophysical Journal, 799, 214

Bond, J. R., Efstathiou, G., Lubin, P. M., & Meinhold, P. R. 1991, Physical Review Letters, 66, 2179

Brodwin, M., Ruel, J., Ade, P. A. R., et al. 2010, The Astrophysical Journal, 721, 90

Connelly, J. L., Wilman, D. J., Finoguenov, A., et al. 2012, The Astrophysical Journal, 756, 139

Evrard, A. E., Bialek, J., Busha, M., et al. 2008, The Astrophysical Journal, 672, 122

Fadda, D., Girardi, M., Iuricin, G., Mardirossian, F., & Mezzetti, M. 1996, The Astrophysical Journal, 473, 670

Gott, J. R. I., & Rees, M. J. 1975, Astronomy and Astrophysics, 45, 365

Hill, G. J., MacQueen, P. J., Smith, M. P., et al. 2008a, in Ground-based and Airborne Instrumentation for Astronomy II. Edited by McLean, ed. I. S. McLean & M. M. Casali, Vol. 7014, 701470–701470–15

Hill, G. J., Gebhardt, K., Komatsu, E., et al. 2008b, Panoramic Views of Galaxy Formation and Evolution ASP Conference Series, 399

Hou, A., Parker, L. C., Harris, W. E., & Wilman, D. J. 2009, The Astrophysical Journal, 702, 1199

Hubble, E., & Humason, M. L. 1931, The Astrophysical Journal, 74, 43

Hubble, E. P. 1926, The Astrophysical Journal, 64, 321

Kravtsov, A. V., & Borgani, S. 2012, Annual Review of Astronomy and Astrophysics, 50, 353

Kurtz, M. J., Mink, D. J., Wyatt, W. F., et al. 1992, Astronomical Data Analysis Software and Systems I, 25

Mehrtens, N., Romer, A. K., Hilton, M., et al. 2012, Monthly Notices of the Royal Astronomical Society, 423, 1024

Munari, E., Biviano, A., Borgani, S., Murante, G., & Fabjan, D. 2013, Monthly Notices of the Royal Astronomical Society, 430, 2638

Murphy, J. D., Gebhardt, K., & Adams, J. J. 2011, The Astrophysical Journal, 729, 129

Murray, S., Power, C., & Robotham, A. 2013, Astronomy and Computing, 3-4, 23

Old, L., Skibba, R. A., Pearce, F. R., et al. 2014, Monthly Notices of the Royal Astronomical Society, 441, 1513

Press, W. H., & Schechter, P. 1974, The Astrophysical Journal, 187, 425

Rozo, E., Rykoff, E. S., Becker, M., Reddick, R. M., & Wechsler, R. H. 2014, eprint arXiv:1410.1193

Ruel, J., Bazin, G., Bayliss, M., et al. 2014, The Astrophysical Journal, 792, 45

Rykoff, E. S., Koester, B. P., Rozo, E., et al. 2012, The Astrophysical Journal, 746, 178

Rykoff, E. S., Rozo, E., Busha, M. T., et al. 2014, The Astrophysical Journal, 785, 104

Sandin, C., Becker, T., Roth, M. M., et al. 2010, Astronomy and Astrophysics, 515, A35

Saro, A., Mohr, J. J., Bazin, G., & Dolag, K. 2013, The Astrophysical Journal, 772, 47

Sehgal, N., Trac, H., Acquaviva, V., et al. 2011, The Astrophysical Journal, 732, 44

Sifón, C., Menanteau, F., Hasselfield, M., et al. 2013, The Astrophysical Journal, 772, 25

Smith, S. 1936, The Astrophysical Journal, 83, 23

Sunyaev, R. A., & Zeldovich, Y. B. 1972, Comments on Astrophysics and Space Physics, 4

The Dark Energy Survey Collaboration. 2005, eprint arXiv:astro-ph/0510346, 42

Tonry, J., & Davis, M. 1979, The Astronomical Journal, 84, 1511

Vanderlinde, K., Crawford, T. M., de Haan, T., et al. 2010, The Astrophysical Journal, 722, 1180

Weinberg, D. H., Mortonson, M. J., Eisenstein, D. J., et al. 2013, Physics Reports, 530, 87

White, S. D. M., & Rees, M. J. 1978, Monthly Notices of the Royal Astronomical Society, 183, 341

Wilman, D. J., Balogh, M. L., Bower, R. G., et al. 2005, Monthly Notices of the Royal Astronomical Society, 358, 71

Zwicky, F. 1933, Helvetica Physica Acta, 6, 110